CHAPTER 15

Novel Graphene Membranes – Theory and Application

Jakob Buchheim[1], Roman M. Wyss[1], Chang-Min Kim[2], Mengmeng Deng[1], Hyung Gyu Park[1]

[1]Department of Mechanical and Process Engineering, Eidgenössische Technische Hochschule (ETH) Zürich, Zürich, Switzerland; [2]School of Environmental Science and Engineering, Gwangju Institute of Science and Technology (GIST), Gwangju, Republic of Korea

15.1 INTRODUCTION

Discovery of the monatomic thickness material graphene has enabled a leap forward in the quest of novel membrane technology research. The two-dimensional (2D) nature of the graphene crystal made of hexagonally arranged, sp2-bonded C atoms [1] exhibits a unique material strength of unmatched stiffness and very high breaking strength [2], rendering graphene a widely studied material not only in solid-state physics but also for membrane applications. The ultimate thinness of the material, in particular, implies promising applications in separation technology. Furthermore, stacked structures of graphene and graphene oxide (GO) offer unique options for tailoring transport selectivity.

15.1.1 Extraordinary Properties of Graphene as a Mass Transport Barrier

One of the most important properties of graphene is its strong diffusion barrier characteristic. It has been found that the defect-free, single crystalline graphene lattice is impermeable to all the gas species, including the smallest monatomic gas He at room temperature energies [3–5]. Furthermore, density functional theory calculations show a potential of selective atomic passage of B, N, H, O in the overall energy barrier order ($\sim 1.3 < 3.2 < 4.2 < 5.5$ eV), with potentially predicting the boron atom passage via an intricate bond switching process that ensues annealing [6]. At room temperature energies, therefore, the 2D carbon crystal does not allow any dissolution of atomic or gas species in the lattice structure, which makes the defect free single-atom-thick graphene an effective barrier for mass transport [7]. For particle energies exceeding room temperature by orders of magnitude, and for such miniscule particles as protons, however, molecular dynamics and experimental findings suggest that particles can indeed penetrate the graphene lattice without causing much damage [8,9].

These extraordinary properties of graphene are currently utilised in corrosion inhibition coatings. Various studies show significant reduction of substrate corrosion when

Emerging Membrane Technology for Sustainable Water Treatment
http://dx.doi.org/10.1016/B978-0-444-63312-5.00015-2

covered by graphene layers [10,11]. For large-scale and polycrystalline graphene coatings, however, grain boundaries and lattice defects impose a weak spot, since the imperfect crystal is prone to permeation of water and gases [12,13]. Localised corrosion damage at graphene grain boundaries [14] could be either patched by atomic layer deposition (ALD) [11] or nullified by multiple layer graphene coating.

15.1.2 Theory of Mass Transport across Thin Membranes

For membrane applications, the exceptional impermeability of defect-free graphene for molecular passage implies a great opportunity to reject media by an atomically thin material. Transport of mass across graphene layers can only occur through artificially created pores and defects. Flow resistance of conventional manifold-type porous filters with thickness, l, is governed by viscous wall friction inside the channels. It is modelled by use of the classic Hagen–Poiseuille flow, a solution of the Navier–Stokes equations that scales the flow rate inversely proportional to l: $Q_{HP} \propto l^{-1}$, where Q_{HP} is the volumetric flow rate. For its atomic thickness, however, porous graphene is expected to impose the lowest possible membrane resistance to mass permeation through a pore of given size in the absence of a channel wall and the associated friction mechanism. For mass transport of a fluid with viscosity, μ, at a differential pressure, Δp, through an orifice with radius, r, in an infinitely thin layer, only the entrance effect dominates the permeation rates by imposing a resistance to the flow. R.A. Sampson found a solution to Stokes flow through such a single orifice [15] which can be extended for a pore array of an infinitely thin disc with porosity, κ, and coefficients $S_3 = 9.03362$, $S_5 = 5.09026$, $S_7 = 4.42312$, $S_9 = 4.19127$ [16]:

$$Q_{\text{Sampson}} = \frac{r^3}{3\mu}\Delta p\left(1 - \frac{2S_3}{3\pi^{5/2}}\kappa^{3/2} - \frac{6S_5}{5\pi^{7/2}}\kappa^{5/2} - \frac{18S_7}{7\pi^{9/2}}\kappa^{7/2} - \frac{56S_9}{9\pi^{11/2}}\kappa^{9/2}\ldots\right)^{-1} \tag{15.1}$$

This entrance effect (or entrance flow resistance) occurs at any pore entrance but is commonly neglected, since the flow resistance caused by the viscous interaction inside the membrane is dominant. In the case of an atomically thin membrane, however, it is no longer negligible. Note that in contrast to the Hagen-Poiseuille flow which scales $Q_{HP} \propto r^4$, the entrance effects is less dependent on the pore diameter since it scales $Q_{\text{Sampson}} \propto r^3$ (Figure 15.1).

For gases where the mean free path, l_{MFP}, of the molecules is larger than the pore diameter ($\text{Kn} = l_{\text{MFP}}/2r > 1$) the mass transport is governed by a free molecular flow theory. Here once again, well-known pore-flow models such as Knudsen diffusion are not applicable for atomically thin porous graphene. It is not the diffusivity of the species inside the pore, which is governed by the pore diameter, that is responsible for the flow impedance [17], but rather the odds of particles entering the pore in the first place. From the basic gas

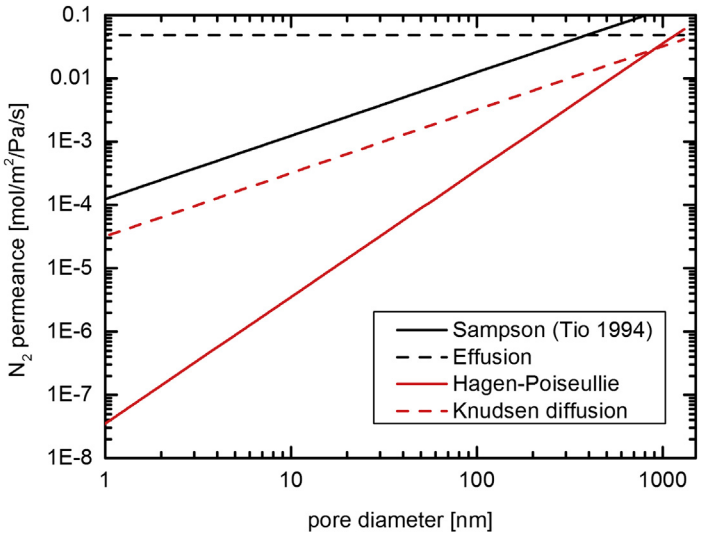

Figure 15.1 Comparison of different pore-flow models. Calculated flux of N_2 at room temperature for various pore sizes. The membrane thickness for conventional pore-flow models (Knudsen diffusion and Hagen–Poiseuille viscous flow) is set to be 2 μm and porosity $\kappa = 0.2$.

kinetic theory, the number of molecules hitting the pore area (πr^2) depends on both the molecular number density, n, and their mean thermal speed in one direction, or $\overline{u}/4$. Molecules on both sides of the membrane hit the pore area, and the net molecular flux across the membrane in thermal equilibrium is determined by the difference in n that can be related to a cross-membrane pressure difference, Δp. As a result, the molecular flow rate takes on the following formula known as effusion theory:

$$\frac{Q_{\text{effusion}}}{V_m} = \pi r^2 \frac{\overline{u}}{4}(n_1 - n_2) = \pi r^2 \frac{\Delta p}{\sqrt{2\pi MRT}} \tag{15.2}$$

where V_m is the molar volume of the transporting species.

The above equation indicates that the flow rate across an infinitely thin separator scales with $Q_{\text{effusion}} \propto r^2$ instead of $Q_{\text{Knudsen}} \propto r^3$, which means that the gas flux (flow rate per unit pore area) in the free molecular flow regime will be independent of the pore size (Figure 15.1).

15.2 POROUS GRAPHENE FLUIDICS – MASS TRANSPORT ACROSS POROUS GRAPHENE

15.2.1 Pore Formation

The idea of an atom-thick membrane platform that can realise non-Fickian transport across a 2D orifice has immediately engendered significant research efforts on large-scale pore formation in the otherwise impermeable graphene. Initial methods of

pore formation in graphene relied on irradiation of freestanding graphene with high-energy electrons inside transmission electron microscopes (TEM). This method allows the formation of a few pores with diameters ranging from 3 Å to 20 nm [18,19]. Since the number of pores created by this method is limited, the technique was only used for solid-state pore sequencing studies [20,21]. For membrane technology applications, however, a larger number of pores have to be created.

One simple way of obtaining a porous graphene membrane is to use graphene synthesised by chemical vapour deposition (CVD). CVD-grown graphene is intrinsically polycrystalline and, therefore, has defect sites along the grain boundaries of individual lattice flakes. Furthermore, it was found that at a certain CVD condition, graphene could form nanometer-scale pinholes ranging from 1 to 15 nm [12] that could be used for mass transport. These pinholes can form if catalyst substrate (e.g. Ni or Cu) has microscale roughness, scratches or surface contamination during growth. At these sites, graphene is hard to nucleate or easily bears many defects.

Artificially made defects in freestanding graphene with subnanometre sizes can be realised by ultraviolet-assisted oxidative etching [22] or direct exposure to ozone [23]. Another technique to create subnanometre pores on graphene is to create sparse lattice defects by low-dose (e.g. 8 keV) Ga^+ ion irradiation followed by weak oxidative etching, based on $KMnO_4$ and H_2SO_4, which grows subnanometre pores from the initially created defect sites [24]. The focused ion beam technology is used to create large-area graphene membranes with controlled pore sizes from micrometres down to a few nanometres via bombardment of high-energy Ga^+ or He^+ ions on freestanding double layer graphene [25]. A parallel process, promising for large-scale pore formation, is the self-assembly-driven nanolithography technique based on block copolymer, which allows the formation of pores of a few tens of nanometres [26]. For subnanometre graphene pores, the tendency of graphene healing has been observed [27], posing a problem regarding long-term membrane stability. In the presence of any C atom supply, graphene tends to reform, and pores vanish. However, atomic-resolution TEM observations have shown that the presence of Si contamination which terminates graphene pore edges could greatly enhance the stability of the pores [28], an idea that might be generalised for the edge stabilisation of graphene pores.

15.2.2 Liquid and Ion Transport through Porous Graphene

15.2.2.1 Theoretical Studies of Water Flow through Porous Graphene

Simulations of liquid flow across porous graphene indicate the high permeation rate of water molecules through such membranes. In molecular dynamics (MD) simulations, Suk and Aluru [29] have predicted ultrahigh permeation of water. For pore sizes around 2.7 nm, the permeance of water molecules through graphene exceeds the mobility inside carbon nanotubes (CNTs) or ultrathin silicon membranes. Only the collective flow of single-file water molecules inside CNT pores of $\sim$0.7 nm is faster than for comparable

pore sizes of graphene. The pressure drop across the graphene pore occurs within ~1 nm from the membrane surface, implying that flow impedance is caused by entrance effects similarly to CNT pores [30].

The effects of pore size and pore edge termination have been further investigated using MD simulations [30]. (Note: The definition of effective pore size may vary in the literature. As the reference points for the measurements, some propose to use the end of the chemical moiety, while others use the centre of the carbon atoms). For pores smaller than 4 nm, the volume flow scaling per pore is roughly $Q \propto r^{3.3}$ [30]. This scaling indicates that water permeance in this pore size regime can be modelled by the superposition of the Sampson and Hagen–Poiseuille formulations. All available results of MD simulations agree roughly with this scaling, $Q \propto r^{x}$, with x lying between 3 and 3.3 [29].

For small pores in the subnanometre range, the edge termination of the graphene pore can influence the permeance [31]. Cohen-Tanugi et al. have found that hydrogenated and hydroxylated groups at the pore mouth have a strong effect. In the pore size range below 1 nm, hydrogen-terminated pores have a slightly lower per-pore permeance than hydroxyl terminated ones of the same pore area [31]. This effect is partially explained by the polar nature of the water molecule, which allows stronger interaction with the hydroxyl group. The latter leads to a larger accessible area inside the hydroxylated pore and, therefore, a larger effective pore size (Figure 15.2). An even stronger effect is that the hydrogen termination renders the pore hydrophobic and, therefore, suppresses

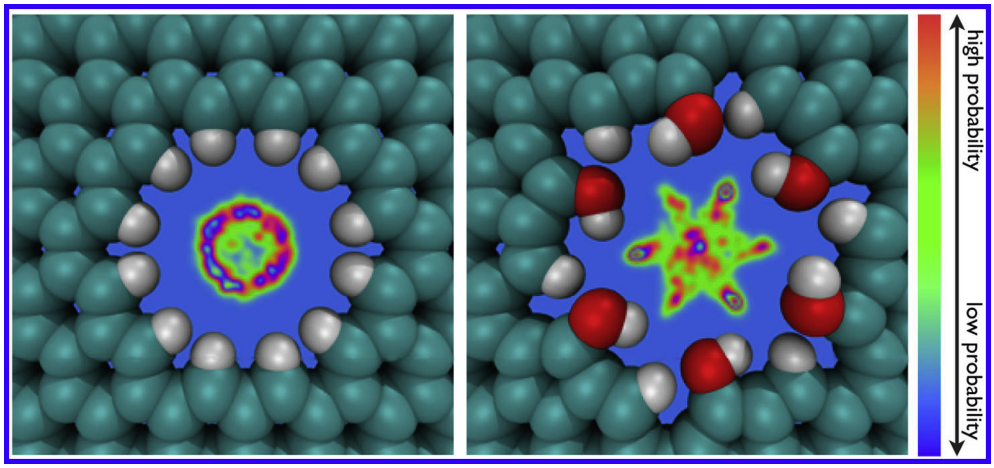

Figure 15.2 Oxygen density maps inside a hydrogenated (left) and hydroxylated pore (right), with open pore areas of 23 Å and 28 Å^2, respectively. Light blue (light grey in print version) indicates the region in which no water oxygens are found, while red (dark grey in print version) regions indicate the highest probability of finding an oxygen atom. *(Ref. [31]. Copyright® (2012) with permission from the American Chemical Society.)*

the formation of hydrogen bonds and reduces the effective pore area. This effect induces an artificial ordering of water molecules in the vicinity of the pore to roughen the entropic landscape and reduces the speed of traversing molecules. In contrast, hydroxylated groups create a smoother landscape for the water molecules, as they can form hydrogen bonds with the water molecules. The overall water flow is therefore increased.

The pore size and pore edge termination also influences the distribution of water molecules inside the pore. By obtaining oxygen density maps [31,32], researchers have observed that, depending on pore size and edge functional groups, the probability density distribution deviates from the homogenous spatial distribution in bulk water (Figure 15.2). Similar to water inside CNTs, water forms layered structures inside the confinement [31,32].

15.2.2.2 Water Permeation Experiments

Water flow across double layer graphene membranes was observed through pore sizes in the range of 50−1000 nm by Celebi, Buchheim et al. [25]. They found that the water flow can only be initiated if both feed and permeate sides of the membrane are pre-wetted by liquid. Otherwise, capillarity prevents the permeation of water through the membrane when only one side is wet, which can counterbalance the driving force of an applied pressure drop to 2 bar or more. The measured per-pore permeance is slightly lower than the theoretical prediction of ultimate permeation but nevertheless matches Sampson's model for scaling of water flow through an orifice with $Q_{H_2O} = (r^3/3\mu_{H_2O})\Delta p$ (Figure 15.3). Despite membrane clogging by particles, the reported flow rate in the case of a 50-nm-pore membrane is almost one order of magnitude higher than for conventional ultrafiltration membranes [25].

The characterisation of liquid flow through graphene membranes was found to be challenging due to clogging of pores with sieved particles and the stability on the support layer [25]. The latter could be improved by attaching the graphene to the support layer with directed Pt deposition, preventing the wash off of the graphene layer (Figure 15.3, inset). Initial attempts to measure water flux across subnanometre pores in graphene [33] lay within the expected ultrahigh flow rate predicted by classic Sampson theory and the MD simulations of Suk and Aluru [30]. By employing a twofold defect sealing method based on ALD to close intrinsic graphene defects and interfacial polymerisation to clog large-scale tears, monolayer graphene could be transformed into a membrane. This allows the measurement of osmotic pressure driven water flux through subnanometre pores. Subnanometre pores are made by defect creation via Ga^+ ion bombardment. This is followed by wet chemical etching (1.875 mM $KMnO_4$ in 6.25% H_2SO_4), resulting in pores of 0.48 nm in diameter. Despite the predictions that this pore size is expected to show ion rejection, NaCl (0.76 nm) passed the membrane favourably. Larger-sized ions and molecules, such as $MgSO_4$ (0.86 nm), Allura Red (~1 nm) and dextran (~3.7 nm), were partly rejected

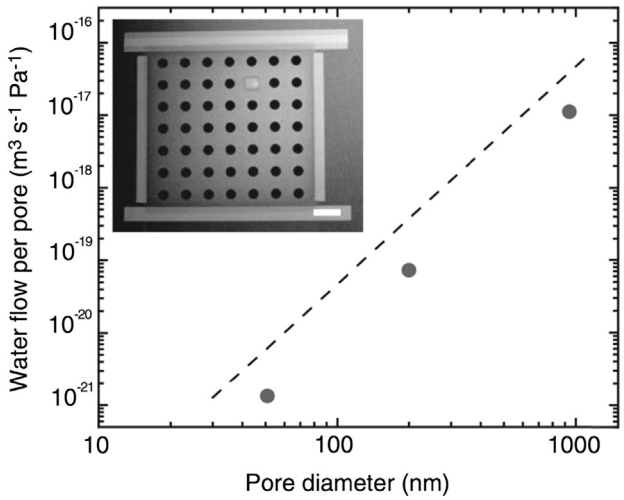

Figure 15.3 Water permeation data: water flow rates per graphene pore for three graphene membranes with different pore sizes, in comparison with the modified Sampson's model prediction (dashed line). (Inset) SEM image of the Pt enclosure surrounding the entire membrane area to prevent membrane disintegration (scale bar, 10 μm). *(Ref. [25]. Copyright® (2014) with permission from the American Association for the Advancement of Science.)*

by the graphene membrane. However, the passage of the dextran molecule and the pumping of NaCl indicate that defect sealing is not perfect, and additional large leakage pathways through the monolayer are present. These, however, could not be found during extensive STEM scanning [33]. The results of this study highlight the difficulty in fabricating defect-free monolayer graphene membranes.

Another method to achieve a water-permeable graphene monolayer was presented by Surwade and coworkers [34]. Monolayer single crystalline graphene covering a 5 μm hole in a SiN_x membrane is treated by oxygen plasma. The exposure generates Si terminated pores with ~1 nm size at pore densities of 10^{14}–10^{16} m^{-2} [34]. Reported results for water permeance are, however, contradicting. Osmotic pressure driven flow through ~1 nm porous graphene yielded $\sim 4.5 \times 10^{-26}$ m^3/Pa/s per pore, which is very close to Sampson's prediction of 6.4×10^{-26} m^3/Pa/s per pore. In a water pervaporation measurement from a closed volume sealed by a graphene membrane at elevated temperatures, the observed water weight loss through the graphene membrane exceeded by orders of magnitude the predicted water permeability of porous graphene for ~20% of the devices. The mechanism for this high permeation rate remains unclear. As expected, in the case of pervaporation, the membrane retains the nonvolatile ions from the passage through the graphene and, therefore, shows some potential application for desalination using graphene membrane [34].

15.2.2.3 Ion Transport through Graphene Pores

MD simulations of ion transport across graphene pores showed the potential of graphene as an ion selective membrane. In one simulation, hydroxyl terminated pores with diameters of ~4 Å allow the passage of Cl^- and Br^- (17:33) but no translocation of F^- or any positively charged ion species [35]. Fluor and nitrogen terminated pores, on the other hand, allowed the passage of K^+, Na^+ and Li^+ at a mobility ratio of 33:14:9. Therefore, two separation mechanisms can be identified: (1) electrostatic screening by the charge of the pore edge functional group rejecting co-ions and (2) steric effects, because ions with weakly bound solvation shells have higher permeation rates than those with strongly solvated ions [35].

Results from MD simulations of graphene pores with hydroxyl dangling bonds, which mimic the structure of K^+ or Na^+ channels, indicate the possibility of ion selective graphene membranes [36]. The pore-mimicking structure of a KcsA K^+ channel showed a K^+ over Na^+ selectivity of 4. Achieving Na^+ selective pores, however, is more challenging. Although the graphene pore, which imitates the NavAB Na^+ channel, preferentially bonds Na^+ to the dangling moiety, the transport path through the pore is too large to block other ions from translocation [36]. Further insight into ion–graphene pore interaction was obtained by equilibrium MD simulations. The concentration, the solvation state and the mobility of K^+ and Cl^- ions inside water-filled graphene pores have been calculated [37]. The concentrations of both ion species in C-terminated graphene pores are reduced in stronger confinement compared to bulk. This is reflected by a low partition coefficient, $\phi = c_p/c_b$, where c_p and c_b denote ion concentrations in graphene pore and bulk, respectively. For pore sizes smaller than 5 Å, c_p (thus ϕ) is practically 0. Suk and Aluru have found that the main factor for the ion partitioning is the high free energy 'cost' for dehydration [37] and not the dielectric exclusion as is the case for conventional nanofiltration membranes [38]. In addition, the diffusion constant D_p of ions inside the graphene confinement is reduced when compared with the bulk diffusion D_{bulk} and scales with pore radius r: $(1/D_p - 1/D_{\text{bulk}}) \propto 1/r$, leading to a remarkable drop of ϕ to ~50% inside a 5.2 Å pore [37].

Experimentally, ion diffusion measurements through graphene with subnanometre pores confirm the potential of ion selectivity and the potential of size exclusion [24]. Pores were created using ion irradiation and wet chemical etching (1.875 mM $KMnO_4$ in 6.25% H_2SO_4), which allowed for control of pore density as well as pore sizes (e.g. by duration of wet chemistry). Short etch times lead to the formation of small pores, which have some preferential selectivity for positively charged K^+ over Cl^-, the latter presumably due to membrane charge. For slightly enlarged pores, K^+ and Cl^- can pass freely but larger dye molecules such as Allura Red (diameter ~1 nm) cannot. Only after opening up the pores further by extended etching times can the dye molecules translocate the pores of the graphene [24]. The ion passage through intrinsic and artificial subnanometre defects was further investigated through ion conductance

measurements [23]. Even mild ozone etching was found to create defects in the range of 3.8 Å, which allow the electrokinetic passage of Na^+ and Cl^- ions. How the electromotive driving force overcomes the dehydration energy penalty of the ions is elusive, but could at least be partly explained if the pore size estimate was offset a little towards smaller values. This report highlights the difficulty in creating nanoporous graphene, as well as correctly characterising the pore.

15.2.2.4 Molecular Dynamics Simulation of Desalination of Water Using Porous Graphene

One of the most important applications of highly water-permeable membranes is seawater desalination. If high water flows can be sustained with high salt rejection, graphene might be an ideal platform for the future desalination processes.

MD simulations of the pressurised flow of high-salinity aqueous NaCl solution through a graphene pore reveal that 100% salt rejection can be achieved for a pore size as narrow as 5.5 Å [31]. This high rejection value for pores <5.5 Å is observed for all pressures from 100 to 225 MPa (Figure 15.4). For larger pores ~9 Å in diameter, the ion rejection is reduced to 80% and 40% at pressures of 100 and 225 MPa, respectively (Figure 15.4). The latter finding is in contrast to the standard diffusive membranes for reverse osmosis desalination [39]. Cohen–Tanugi and Grossman [31] argue that the large effective volume of the hydrated ion is more sensitive to pressure increase than water molecules. Furthermore, a clear effect of pore edge chemistry is observed. Pores

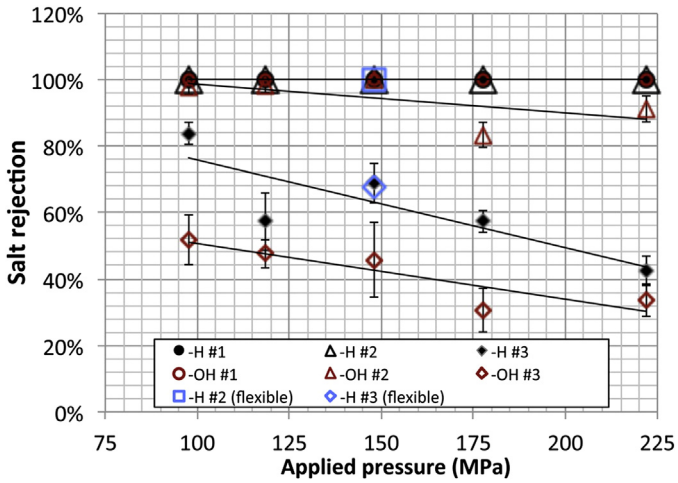

Figure 15.4 Average salt rejection as a function of pore type and pressure differential. The results indicate that smaller pores are capable of effectively rejecting salt, but that rejection performance decreases with higher pressures. Moreover, hydrogenated pores exhibit a stronger salt rejection performance than hydroxylated ones. *(Ref. [31]. Copyright® (2012) with permission from the American Chemical Society.)*

that are terminated by the polar hydroxylated group allow higher salt permeation (lower salt rejection). The OH group on the pore edge interacts in a similar way with the solvated ion as do the surrounding water molecules and, therefore, the energy barrier for ion passage may be lower [31]. In contrast, hydrogen-terminated pores show greater ion separation performance, with up to 80% for ~8 Å pores at 100 MPa.

Equilibrium MD simulations give further insights into the potential mean force (PMF) acting on the water molecules and ions at the graphene pore [40]. Na^+ ions and Cl^- have to overcome the PMF barrier of ~0.61 and ~0.43 eV in passing a nonfunctionalised graphene pore of 7.5 Å in diameter. On the other hand, water molecules face a PMF barrier of only ~0.2 eV [40]. Larger pristine graphene pores are not expected to show a significant ion rejection. In addition, changes in salinity from 0.025 to 0.25 M do not change the PMF barrier significantly for nonfunctionalised graphene pores. In contrast, the PMF barrier of functionalised graphene pores changes with the salinity of the electrolyte solution. The case of pore edge chemistry modification by the attachment of carboxylic groups increases the PMF for Cl^- at low ionic strength to 0.824 eV. However, at high ionic strength, the increased Na^+ ion concentration at the pore screens the electrostatic repulsive barrier of Cl^-, yielding a lower PMF for the Cl^- ion passage of ~0.47 eV. The attachment of a NH_3 group causes the same but reverse effect on both ion species, so that the overall passage of ions is not expected to decrease [40]. In contrast, the functionalisation of the pore edge with OH groups has beneficial effects on the salt rejection performance, since it allows for high salt rejection, even for salinities as high as those encountered in seawater [40].

One important additional factor for seawater desalination is the mechanical strength of the graphene membrane [41]. Typical hydraulic pressures for the reverse osmosis process range from 5 to 10 MPa (50–100 bar). In order to achieve a high throughput of permeate (desalinated water), membranes need to sustain similar mechanical pressures. The mechanical strength of nonporous, monocrystalline graphene (with a Young's Modulus of 1 TPa) indicates that graphene can indeed withstand high pressures. Simulations have shown that porous graphene can sustain around 57 MPa if the support dimensions are carefully selected [41].

15.3 MASS TRANSPORT ACROSS LAYERED GRAPHENE AND GRAPHENE OXIDE

15.3.1 Gas Separation

While nanometre-scale perforation is needed to impart permeation to the otherwise impermeable 2D material, staggered stacking of 2D material platelets layer-by-layer can potentially create molecular transport pathways in a meandering fashion. Graphene-based 2D platelets can be formed in various methods, posing highly graphitic surfaces and chemically derived surfaces. Stacked pure graphene platelets incorporate

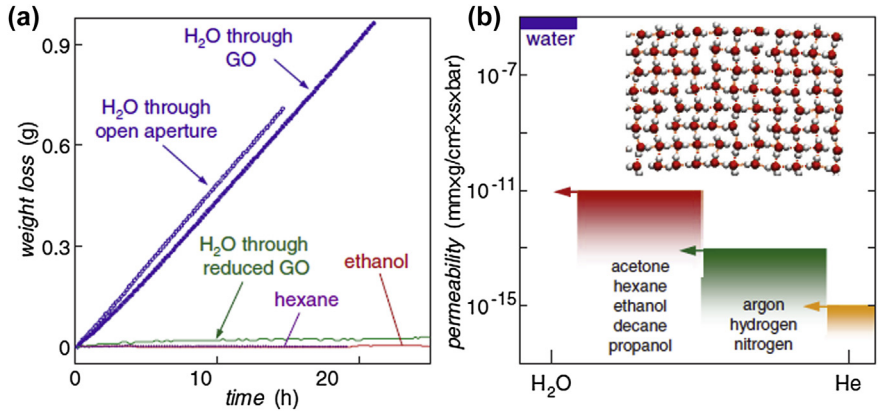

Figure 15.5 Permeation through graphene oxide (GO). (a) Weight loss for a container sealed with a GO film (aperture area ≈ 1 cm^2). No loss was detected for ethanol, hexane, etc., but water evaporated from the container as freely as through an open aperture (blue (grey in print version) curves). The measurements were carried out at room temperature in zero humidity. (b) Permeability of GO paper with respect to water and various small molecules (arrows indicate the upper limits set by experiments). (Inset) Schematic representation of the structure of monolayer water inside a graphene capillary with $d = 7$ Å. *(Ref. [42]. Copyright® (2012) with permission from the American Association for the Advancement of Science.)*

van der Waals interactions, impeding molecular passage in between them. On the other hand, chemically derived platelets, called GO, could allow for the construction of molecular pillars in between the platelets during the packing process to open up space for molecular passage.

The permeation rate of water vapour through thick GO laminates (from 0.1 to 10 μm) was reported to be similar to the evaporation rate from an open water surface under similar conditions (Figure 15.5(a)). In addition, it showed highly selective transport only for water molecules whereas even smaller He molecules cannot be transmitted (Figure 15.5(b)). This observation indicates that water molecules can pass through nanochannels formed between GO platelets interacting strongly with them [42]. The observation has triggered a wide area of research and development, since the mass transport through the nanochannel can occur selectively, and simple stacking of GO sheets is considered a facile way to prepare selective and ultrathin membranes. For gas separation, the permeance of the GO membrane is affected by preparation methods. It is the stacking method or layer-interlocking strategy that has a great influence on both the gas permeability and selectivity of the GO membranes. The gas selectivity in particular can be roughly explained by a kinetic diameter argument (Figure 15.6). Therefore, it is believed that the gas separation mechanism of GO membranes is primarily molecular sieving. However, permeances of some gases deviate from those predictions employing the kinetic diameters, calling for further investigations [43,44].

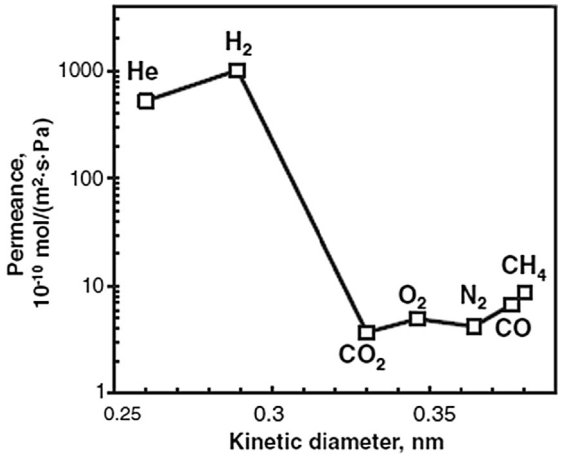

Figure 15.6 Single-gas permeation through graphene oxide (GO) membranes supported on porous alumina membrane at 20 °C. Permeances of seven molecules through a ~18-nm-thick GO membrane. *(Ref. [44]. Copyright® (2013) with permission from the American Association for the Advancement of Science.)*

15.3.2 Water Permeation and Separation

For the purpose of nanofiltration, base-refluxing-reduced GO is supported by an anodic aluminium oxide substrate. The rejection for small ions such as NaCl, Na_2SO_4, $MgCl_2$ and $MgSO_4$ was less than 60%, but for large molecules (i.e. methyl blue and direct red 81) the rejection was higher than 99% with a higher water flux than that of a commercial polymer nanofiltration membrane (Table 15.1). The electrostatic interaction between

Table 15.1 Retention of organic dyes for ultrathin graphene nanofiltration membranes (uGNM) with different base-refluxing-reduced GO (brGO) loadings and brGO layer thickness

brGO loading (mg/m^2)	Thickness (nm)	Pure water flux j_0 (L/m^2/h/bar)	MB[a]			DR 81[a]		
			Retention (%)	J/J_0 (%)[b]	C/C_0[c]	Retention (%)	J/J_0 (%)[b]	C/C_0[c]
14.1[d]	22	21.81	99.2	90.0	1.27	99.9	89.6	1.31
17.0[c]	26	12.62	99.7	91.1	1.30	99.8	89.7	1.33
21.2[e]	33	5.00	99.7	89.4	1.32	99.9	87.2	1.33
28.3[e]	44	4.37	99.6	90.4	1.33	99.9	95.8	1.34
34.0[e]	53	3.26	99.8	95.0	1.36	99.9	95.6	1.35

[a]The concentration of feed dye solution C_0 was 0.002 mM.
[b]The ratio of permeate flux of the dye solution J to the pure water flux J_0.
[c]Concentration ratio of upper stream (C) when the permeation volume was 10 mL to the original feeding solution (C_0 35 mL).
[d]The applied pressure was 1 bar.
[e]The applied pressure was 5 bar.
Ref. [45]. Copyright® (2013) with permission from Wiley-VCH.

a graphene membrane and solutes can be explained with the Gibbs—Donnan equilibrium theory [45]; the size exclusion or the steric hindrance mechanism is under active investigation in the research community.

GO flakes and stacked membranes made out of them are prone to dispersion and disassembly in an aqueous environment, raising concerns about long-term stability as a water purification membrane material [46]. As one way to tackle this problem of membrane disintegration, polydopamine was used to bridge GO flakes and offer support, and 1,3,5-benzenetricarbonyl trichloride was also employed to make a chemical bonding between GO flakes. The water permeability was measured to be 8—27.6 $L/m^2/h/bar$. The GO membrane showed a high rejection rate (>93% for Rhodamine WT) for large organic molecules, whereas the rejection for ions was relatively low (6—19% for NaCl) when the system was pressurised. Interestingly, both water flux and salt rejection were not a strong function of the number of GO layers, implying that even a very thin GO membrane could in principle separate ions and organic matter in water. In addition, the rejection of ions decreased with increase in concentration of the ions, which was attributed to the change of Debye length and is partly supportive of the charge exclusion mechanism [47].

In contrast with the assertion of previous reports, if GO is placed on alumina filters during the preparation method of vacuum filtration, membranes show stability in water without the need for any bonding agent between GO platelets or between GO flakes and substrate. The micrometres-thick GO membranes prepared in this way have shown selective transport towards water only, a similar result to water vapour transport across thick GO membranes. Ions with large-hydrated radii can be separated via size exclusion. The charge of ions or molecules, however, did not play a decisive role in the separation, which is supported by an observation that the rate of permeation of AsO_4^{3-} was almost identical to that of Na^+ or Cl^- [48]. This observation hints that electrostatic interaction may become much weakened in a so-called charge neutralisation environment between GO and alumina cations.

Forward osmosis (FO) is another application of the stacked 2D membranes. For an FO process, a freestanding reduced GO (rGO) membrane has shown a promising result. Freestanding rGO membranes show higher flux (57.0 $L/m^2/h$ when deionised water and NaCl (2.0 M) were used as feed and draw solutions, respectively) than a commercial FO membrane (CTA membrane, ~10 $L/m^2/h$ at the same conditions) (Figure 15.7(a)). This finding is particularly important because freestanding rGO membranes could eliminate the problematic issue of an internal concentration polarisation in the FO process, allowing an increase in apparent chemical potential — and hence osmotic pressure — difference (Figure 15.7(b)). Importantly, the reverse salt flux in $g/m^2/h$ is lower, and the salt rejection capability of the rGO membrane is higher, than that of the CTA membrane (Figure 15.7(c) and (d)) [49].

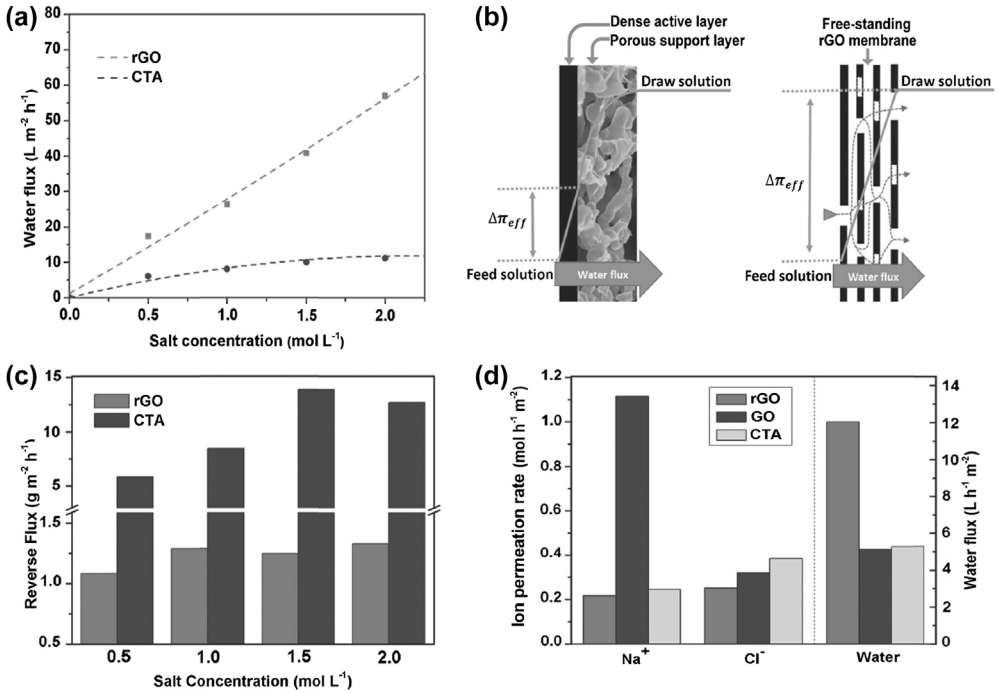

Figure 15.7 Forward osmosis (FO) test of the freestanding reduced graphene oxide (rGO) membrane. (a) Variation of water fluxes of the freestanding rGO (100 nm thick) and commercial hydration technology innovations (HTI) CTA membranes as a function of salt (draw solution) concentrations. (b) Comparison of the osmotic pressure profiles for the conventional supported membrane (left) and freestanding rGO (right) membrane in the FO process. For rGO membranes, the intrinsic defects (i.e. holes and wrinkles) act as the channels for mass transport. (c) Variations of reverse salt flux of the freestanding rGO (100 nm thick) and commercial HTI CTA membranes as a function of salt (draw solution) concentrations. (d) Permeation rates of Na^+ and Cl^- and water fluxes through rGO, GO and CTA membranes using NaCl as feed solution and ammonia as draw solution, respectively. *(Source: Ref. [49]. Copyright® (2014) with permission from Wiley-VCH.)*

15.3.3 Theoretical Investigation

Theoretical modelling may be able to explain the origin of the superior performance of these stacked graphene structures as well as identify new operations and applications. Based on first principle simulation, the ultrafast permeation of water across the stacked graphene structure has been attributed to the unique hydrogen bonding (HB) configuration under the tight nanoscale 2D confinements. Even though the interlayer distance was narrowed to 10 Å, the average HB per water molecule is comparable to that of bulk water. However, the effect of perturbation appears to be localised only at the graphene–water interface, thereby weakening the molecular dipole moments and HBs at the interface and changing the tilting angle of water. As a result, the water mobility can be enhanced in this nanometre-confined environment [50].

On the other hand, phase inversion of water molecules from liquid to solid (ice) in the nanoconfined 2D channel was suspected as a major reason for the anomalous transport of water through the stacked graphene channels. Unlike other molecules, such as He, Ar, N_2 and H_2, only water molecules can change their phase in the highly confined graphitic channel because of the unique HB configuration of water. The long-range order of the ice form is energetically favoured much more than liquid water inside the 2D confinement. Thus, the formation of ice will facilitate collective motion of water in between graphene layers with less friction and render an easy passage of water through the stacked graphene layers. According to the simulation results, an ice bilayer forms at an optimal interlayer distance (7−10 Å) more favourably than an ice monolayer, explained by the lower energy barriers of the ice bilayer [51].

Molecular slip flow within the stacked graphene structure has been proven possible by theoretical investigations. Because of the intrinsic smoothness and ordered crystal structure of graphene, molecules could slide over the graphene sheet easily. Comparison of the slip lengths of other liquid species (i.e. Ar and CH_4) with water revealed that water has a much longer slip length, regardless of the flow regime. The slip lengths for Ar and CH_4 liquids were 11 ± 1 nm and 5.9 ± 0.6 nm, respectively, while that of water was 60 ± 6 nm [52].

The ultrafast and highly selective transport properties exhibited by the stacked graphene structure are an outcome of nanometre-sized tight confinement, the special properties of graphene and the properties of the fluid confined in it. In particular, water in both the liquid and gas phase has shown a unique behaviour distinct from other species. The stacked graphene structure has great potential for further fundamental investigation and applications in various areas, which demand high-performance standards in selectivity and permeation.

15.4 CONCLUSIONS

For water purification technology, high permeance and great selectivity are the primary properties desired for general filtration membrane materials; these properties, however, tend to counteract each other to form a trade-off. Porous graphene, a perforated membrane made out of mono- or few-layer graphene, can be mechanically robust and offer ultimate permeation to a transport species. It indicates potential for water purification and seawater desalination if the perforation is executed with sub-2 nanometre precision and at maximal areal porosity. The edge chemistry of the pores has a significant role in imparting pronounced selectivity to the membrane and also influences the permeance of pure water through the membrane. Stacked graphene platelets offer another filtration membrane architecture. They can be made sturdy in aqueous environments by various self-adhering methods and offer great selectivity towards water and weakly charged small ions. Selectivity of the stacked GO platelet

membrane is controllable by tailoring the layer-by-layer distance with chemical reduction and oxidation and is governed by charge-based exclusion, size exclusion and steric hindrance.

Porous 2D layer and stacked platelets are two potential designs for embodying ultrapermeable and highly selective membranes, respectively. If combined in a rational design, a synergistic membrane architecture for an extremely efficient water treatment could be obtained. To this end, a great deal of experimental and theoretical investigation needs to be performed to fully understand the materials as well as the transport and selection mechanisms, and also to further develop manufacturing options.

REFERENCES

[1] K.S. Novoselov, A.K. Geim, S.V. Morozov, D. Jiang, Y. Zhang, S.V. Dubonos, I.V. Grigorieva, A.A. Firsov, Electric field effect in atomically thin carbon films, Science 306 (2004) 666–669.
[2] C. Lee, X. Wei, J.W. Kysar, J. Hone, Measurement of the Elastic Properties and Intrinsic Strength of Monolayer Graphene, Science 321 (2008) 385–388.
[3] O. Leenaerts, B. Partoens, F.M. Peeters, Graphene: a perfect nanoballoon, Applied Physics Letters 93 (2008) 193107.
[4] J.S. Bunch, S.S. Verbridge, J.S. Alden, A.M. Van Der Zande, J.M. Parpia, H.G. Craighead, P.L. McEuen, Impermeable atomic membranes from graphene sheets, Nano Letters 8 (2008) 2458–2462.
[5] T. Georgiou, L. Britnell, P. Blake, R.V. Gorbachev, A. Gholinia, A.K. Geim, C. Casiraghi, K.S. Novoselov, Graphene bubbles with controllable curvature, Applied Physics Letters 99 (2011) 093103.
[6] L. Tsetseris, S.T. Pantelides, Graphene: an impermeable or selectively permeable membrane for atomic species? Carbon 67 (2014) 58–63.
[7] V. Berry, Impermeability of graphene and its applications, Carbon 62 (2013) 1–10.
[8] O. Lehtinen, J. Kotakoski, A.V. Krasheninnikov, A. Tolvanen, K. Nordlund, J. Keinonen, Effects of ion bombardment on a two-dimensional target: atomistic simulations of graphene irradiation, Physical Review B: Condensed Matter and Materials Physics 81 (2010) 153401.
[9] S. Hu, M. Lozada-Hidalgo, F.C. Wang, A. Mishchenko, F. Schedin, R.R. Nair, E.W. Hill, D.W. Boukhvalov, M.I. Katsnelson, R.A. Dryfe, I.V. Grigorieva, H.A. Wu, A.K. Geim, Proton transport through one-atom-thick crystals, Nature 516 (2014) 227–230.
[10] S. Chen, L. Brown, M. Levendorf, W. Cai, S.-Y. Ju, J. Edgeworth, X. Li, C.W. Magnuson, A. Velamakanni, R.D. Piner, J. Kang, J. Park, R.S. Ruoff, Oxidation resistance of graphene-coated Cu and Cu/Ni alloy, ACS Nano 5 (2011) 1321–1327.
[11] Y.-P. Hsieh, M. Hofmann, K.-W. Chang, J.G. Jhu, Y.-Y. Li, K.Y. Chen, C.C. Yang, W.-S. Chang, L.-C. Chen, Complete corrosion inhibition through graphene defect passivation, ACS Nano 8 (2014) 443–448.
[12] S.C. O'Hern, C.A. Stewart, M.S.H. Boutilier, J.-C. Idrobo, S. Bhaviripudi, S.K. Das, J. Kong, T. Laoui, M. Atieh, R. Karnik, Selective molecular transport through intrinsic defects in a single layer of CVD graphene, ACS Nano 6 (2012) 10130–10138.
[13] T. Yoon, J.H. Mun, B.J. Cho, T.S. Kim, Penetration and lateral diffusion characteristics of polycrystalline graphene barriers, Nanoscale 6 (2014) 151–156.
[14] M. Schriver, W. Regan, W.J. Gannett, A.M. Zaniewski, M.F. Crommie, A. Zettl, Graphene as a long-term metal oxidation barrier: worse than nothing, ACS Nano 7 (2013) 5763–5768.
[15] R.A. Sampson, On Stokes's current function, Philosophical Transactions of the Royal Society of London A (1891) 449–518.

[16] K.-K. Tio, S.S. Sadhal, Boundary conditions for Stokes flows near a porous membrane, Applied Science Research 52 (1994) 1–20.
[17] M. Knudsen, Die Molekularströmung der Gase durch Öffnungen und die Effusion, Annals of Physics 333 (1909) 999–1016.
[18] M.D. Fischbein, M. Drndić, Electron beam nanosculpting of suspended graphene sheets, Applied Physics Letters 93 (2008) 113107.
[19] C.J. Russo, J.A. Golovchenko, Atom-by-atom nucleation and growth of graphene nanopores, Proceedings of the National Academy of Science of the United State of America 109 (2012) 5953–5957.
[20] C.A. Merchant, K. Healy, M. Wanunu, V. Ray, N. Peterman, J. Bartel, M.D. Fischbein, K. Venta, Z. Luo, A.T.C. Johnson, M. Drndic, DNA translocation through graphene nanopores, Nano Letters 10 (2010) 2915–2921.
[21] G.F. Schneider, S.W. Kowalczyk, V.E. Calado, G. Pandraud, H.W. Zandbergen, L.M.K. Vandersypen, C. Dekker, DNA translocation through graphene nanopores, Nano Letters 10 (2010) 3163–3167.
[22] S.P. Koenig, L. Wang, J. Pellegrino, J.S. Bunch, Selective molecular sieving through porous graphene, Nature Nanotechnology 7 (2012) 728–732.
[23] M.I. Walker, R.S. Weatherup, N.A.W. Bell, S. Hofmann, U.F. Keyser, Free-standing graphene membranes on glass nanopores for ionic current measurements, Applied Physics Letters 106 (2015) 023119.
[24] S.C. O'Hern, M.S. Boutilier, J.C. Idrobo, Y. Song, J. Kong, T. Laoui, M. Atieh, R. Karnik, Selective ionic transport through tunable subnanometer pores in single-layer graphene membranes, Nano Letters 14 (2014) 1234–1241.
[25] K. Celebi, J. Buchheim, R.M. Wyss, A. Droudian, P. Gasser, I. Shorubalko, J.I. Kye, C. Lee, H.G. Park, Ultimate permeation across atomically thin porous graphene, Science 344 (2014) 289–292.
[26] J. Bai, X. Zhong, S. Jiang, Y. Huang, X. Duan, Graphene nanomesh, Nature Nanotechnology 5 (2010) 190–194.
[27] R. Zan, Q.M. Ramasse, U. Bangert, K.S. Novoselov, Graphene reknits its holes, Nano Letters 12 (2012) 3936–3940.
[28] J. Lee, Z. Yang, W. Zhou, S.J. Pennycook, S.T. Pantelides, M.F. Chisholm, Stabilization of graphene nanopore, Proceedings of the National Academy of Sciences of the United States of America 111 (2014) 7522–7526.
[29] M.E. Suk, N.R. Aluru, Water transport through ultrathin graphene, The Journal of Physical Chemistry Letters 1 (2010) 1590–1594.
[30] M.E. Suk, N.R. Aluru, Molecular and continuum hydrodynamics in graphene nanopores, RSC Advances 3 (2013) 9365–9372.
[31] D. Cohen-Tanugi, J.C. Grossman, Water desalination across nanoporous graphene, Nano Letters 12 (2012) 3602–3608.
[32] C. Zhu, H. Li, S. Meng, Transport behavior of water molecules through two-dimensional nanopores, Journal of Chemical Physics 141 (2014) 18C528.
[33] S.C. O'Hern, D. Jang, S. Bose, J.C. Idrobo, Y. Song, T. Laoui, J. Kong, R. Karnik, Nanofiltration across defect-sealed nanoporous monolayer graphene, Nano Letters 15 (2015) 3254–3260.
[34] S.P. Surwade, S.N. Smirnov, I.V. Vlassiouk, R.R. Unocic, G.M. Veith, S. Dai, S.M. Mahurin, Water desalination using nanoporous single-layer graphene, Nature Nanotechnology 10 (2015) 459–464.
[35] K. Sint, B. Wang, P. Král, Selective ion passage through functionalized graphene nanopores, Journal of the American Chemical Society 130 (2008) 16448–16449.
[36] Z. He, J. Zhou, X. Lu, B. Corry, Bioinspired graphene nanopores with voltage-tunable ion selectivity for Na^+ and K^+, ACS Nano 7 (2013) 10148–10157.
[37] M.E. Suk, N.R. Aluru, Ion transport in sub-5-nm graphene nanopores, Journal of Chemical Physics 140 (2014) 084707.
[38] A.E. Yaroshchuk, Dielectric exclusion of ions from membranes, Advances in Colloid and Interface Science 85 (2000) 193–230.
[39] M.E. Williams, A Review of Reverse Osmosis Theory, EET Corporation and Williams Engineering Services Company Inc., 2003.

[40] D. Konatham, J. Yu, T.A. Ho, A. Striolo, Simulation insights for graphene-based water desalination membranes, Langmuir 29 (2013) 11884–11897.
[41] D. Cohen-Tanugi, J.C. Grossman, Mechanical strength of nanoporous graphene as a desalination membrane, Nano Letters 14 (2014) 6171–6178.
[42] R.R. Nair, H.A. Wu, P.N. Jayaram, I.V. Grigorieva, A.K. Geim, Unimpeded permeation of water through helium-leak-tight graphene-based membranes, Science 335 (2012) 442–444.
[43] H.W. Kim, H.W. Yoon, S.M. Yoon, B.M. Yoo, B.K. Ahn, Y.H. Cho, H.J. Shin, H. Yang, U. Paik, S. Kwon, J.Y. Choi, H.B. Park, Selective gas transport through few-layered graphene and graphene oxide membranes, Science 342 (2013) 91–95.
[44] H. Li, Z. Song, X. Zhang, Y. Huang, S. Li, Y. Mao, H.J. Ploehn, Y. Bao, M. Yu, Ultrathin, molecular-sieving graphene oxide membranes for selective hydrogen separation, Science 342 (2013) 95–98.
[45] Y. Han, Z. Xu, C. Gao, Ultrathin graphene nanofiltration membrane for water purification, Advanced Functional Materials 23 (2013) 3693–3700.
[46] C.N. Yeh, K. Raidongia, J.J. Shao, Q.H. Yang, J.X. Huang, On the origin of the stability of graphene oxide membranes in water, Nature Chemistry 7 (2015) 166–170.
[47] M. Hu, B. Mi, Enabling graphene oxide nanosheets as water separation membranes, Environmental Science & Technology 47 (2013) 3715–3723.
[48] R.K. Joshi, P. Carbone, F.C. Wang, V.G. Kravets, Y. Su, I.V. Grigorieva, H.A. Wu, A.K. Geim, R.R. Nair, Precise and ultrafast molecular sieving through graphene oxide membranes, Science 343 (2014) 752–754.
[49] H. Liu, H. Wang, X. Zhang, Facile fabrication of freestanding ultrathin reduced graphene oxide membranes for water purification, Advanced Materials 27 (2015) 249–254.
[50] G. Cicero, J.C. Grossman, E. Schwegler, F. Gygi, G. Galli, Water confined in nanotubes and between graphene sheets: a first principle study, Journal of the American Chemical Society 130 (2008) 1871–1878.
[51] D.W. Boukhvalov, M.I. Katsnelson, Y.W. Son, Origin of anomalous water permeation through graphene oxide membrane, Nano Letters 13 (2013) 3930–3935.
[52] S.K. Kannam, B.D. Todd, J.S. Hansen, P.J. Daivis, Slip flow in graphene nanochannels, Journal of Chemical Physics 135 (2011) 144701.